
An Investigation into Whitening Loss for Self-supervised Learning

Xi Weng^{*1}, Lei Huang^{*✉ 1,2}, Lei Zhao^{*1},
Rao Muhammad Anwer², Salman Khan², Fahad Shahbaz Khan²

¹SKLSDE, Institute of Artificial Intelligence, Beihang University, Beijing, China

²Mohamed bin Zayed University of Artificial Intelligence, UAE

Abstract

A desirable objective in self-supervised learning (SSL) is to avoid feature collapse. Whitening loss guarantees collapse avoidance by minimizing the distance between embeddings of positive pairs under the conditioning that the embeddings from different views are whitened. In this paper, we propose a framework with an informative indicator to analyze whitening loss, which provides a clue to demystify several interesting phenomena as well as a pivoting point connecting to other SSL methods. We reveal that batch whitening (BW) based methods do not impose whitening constraints on the embedding, but they only require the embedding to be full-rank. This full-rank constraint is also sufficient to avoid dimensional collapse. Based on our analysis, we propose channel whitening with random group partition (CW-RGP), which exploits the advantages of BW-based methods in preventing collapse and avoids their disadvantages requiring large batch size. Experimental results on ImageNet classification and COCO object detection reveal that the proposed CW-RGP possesses a promising potential for learning good representations. The code is available at <https://github.com/winci-ai/CW-RGP>.

1 Introduction

Self-supervised learning (SSL) has made significant progress over the last several years [1, 21, 6, 18, 8], almost reaching the performance of supervised baselines on many downstream tasks [36, 27, 38]. Several recent approaches rely on a joint embedding architecture in which a dual pair of networks are trained to produce similar embeddings for different views of the same image [8]. Such methods aim to learn representations that are invariant to transformation of the same input. One main challenge with the joint embedding architectures is how to prevent a *collapse* of representation, in which the two branches ignore the inputs and produce identical and constant output representations [6, 8].

One line of work uses contrastive learning methods that attract different views from the same image (positive pairs) while pull apart different images (negative pairs), which can prevent constant outputs from the solution space [47]. While the concept is simple, these methods need large batch size to obtain a good performance [21, 6, 40]. Another line of work tries to directly match the positive targets without introducing negative pairs. A seminal approach, BYOL [18], shows that an extra predictor and momentum is essential for representation learning. SimSiam [8] further generalizes [18] by empirically showing that stop-gradient is essential for preventing trivial solutions. Recent works generalize the collapse problem into *dimensional collapse* [24, 28]² where the embedding vectors only span a lower-dimensional subspace and would be highly correlated. Therefore, the embedding vector dimensions would vary together and contain redundant information. To prevent the *dimensional*

^{*}equal contribution [✉]corresponding author (huangleiAI@buaa.edu.cn). This work was partially done while Lei Huang was a visiting scholar at Mohamed bin Zayed University of Artificial Intelligence, UAE.

²This collapse is also referred to *informational collapse* in [2].

collapse, whitening loss is proposed by only minimizing the distance between embeddings of positive pairs under the condition that embeddings from different views are whitened [13, 24]. A typical way is using batch whitening (BW) and imposing the loss on the whitened output [13, 24], which obtains promising results.

Although whitening loss has theoretical guarantee in avoiding collapse, we experimentally observe that this guarantee depends on which kind of whitening transformation [29] is used in practice (see Section 3.2 for details). This interesting observation challenges the motivations of whitening loss for SSL. Besides, the motivation of whitening loss is that the whitening operation can remove the correlation among axes [24] and a whitened representation ensures the examples scattered in a spherical distribution [13]. Based on this argument, one can use the whitened output as the representation for downstream tasks, but it is not used in practice. To this end, this paper investigates whitening loss and tries to demystify these interesting observations. Our contributions are as follows:

- We decompose the symmetric formulation of whitening loss into two asymmetric losses, where each asymmetric loss requires an online network to match a whitened target. This mechanism provides a pivoting point connecting to other methods, and a way to understand why certain whitening transformation fails to avoid *dimensional collapse*.
- Our analysis shows that BW based methods do not impose whitening constraints on the embedding, but they only require the embedding to be full-rank. This full-rank constraint is also sufficient to avoid *dimensional collapse*.
- We propose channel whitening with random group partition (CW-RGP), which exploits the advantages of BW-based method in preventing collapse and avoids their disadvantages requiring large batch size. Experimental results on ImageNet classification and COCO object detection show that CW-RGP has promising potential in learning good representation.

2 Related Work

A desirable objective in self-supervised learning is to avoid feature collapse.

Contrastive learning prevents collapse by attracting positive samples closer, and spreading negative samples apart [47, 48]. In these methods, negative samples play an important role and need to be well designed [37, 1, 23]. One typical mechanism is building a memory bank with a momentum encoder to provide consistent negative samples, proposed in MoCos [21], yielding promising results [21, 7, 9, 33]. Other works include SimCLR [6] addresses that more negative samples in a batch with strong data augmentations perform better. Contrastive methods require large batch sizes or memory banks, which tends to be costly, promoting the questions whether negative pairs is necessary.

Non-contrastive methods aim to accomplish SSL without introducing negative pairs explicitly [3, 4, 34, 18, 8]. One typical way to avoid representational collapse is the introduction of asymmetric network architecture. BYOL [18] appends a predictor after the online network and introduce momentum into the target network. SimSiam [8] further simplifies BYOL by removing the momentum mechanism, and shows that stop-gradient to target network serves as an alternative approximation to the momentum encoder. Other progress includes an asymmetric pipeline with a self-distillation loss for Vision Transformers [5]. It remains not clear how the asymmetric network avoids collapse without negative pairs, leaving the debates on batch normalization (BN) [15, 45, 39] and stop-gradient [8, 50], even though preliminary works have attempted to analyze the training dynamics theoretical with certain assumptions [44] and build a connection between asymmetric network with contrastive learning methods [42]. Our work provides a pivoting point connecting asymmetric network to profound whitening loss in avoiding collapse.

Whitening loss has theoretical guarantee in avoiding collapse by minimizing the distance of positive pairs under the conditioning that the embeddings from different views are whitened [49, 13, 24, 2]. One way to obtain whitened output is imposing a whitening penalty as regularization on embedding—the so-called soft whitening, which is proposed in Barlow Twins [49], VICReg [2] and CCA-SSG [51]. Another way is using batch whitening (BW) [25]—the so-called hard whitening, which is used in W-MSE [13] and Shuffled-DBN [24]. We propose a different hard whitening method—channel whitening (CW) that has the same function that ensures all the singular values of transformed output being one for avoiding collapse. But CW is more numerical stable and works better when batch size is small, compared to BW. Furthermore, our CW with random group partition (CW-RGP) can effectively control the extent of constraint on embedding and obtain better performance in practice. We note that a recent work ICL [52] proposes to decorrelate instances, like CW but having several significant

differences in technical details. ICL uses "stop-gradient" for the whitening matrix, while CW requires back-propagation through the whitening transformation. Besides, ICL uses extra pre-conditioning on the covariance and whitening matrices, which is essential for the numerical stability, while CW does not use extra pre-conditioning and can work well since it encourages the embedding to be full-rank.

3 Exploring Whitening Loss for SSL

3.1 Preliminaries

Let \mathbf{x} denote the input sampled uniformly from a set of images \mathbb{D} , and \mathbb{T} denote the set of data transformations available for augmentation. We consider the Siamese network $f_\theta(\cdot)$ parameterized by θ . It takes as input two randomly augmented views, $\mathbf{x}_1 = \mathcal{T}_1(\mathbf{x})$ and $\mathbf{x}_2 = \mathcal{T}_2(\mathbf{x})$, where $\mathcal{T}_{1,2} \in \mathbb{T}$. The network $f_\theta(\cdot)$ is trained with an objective function that minimizes the distance between embeddings obtained from different views of the same image:

$$\mathcal{L}(\mathbf{x}, \theta) = \mathbb{E}_{\mathbf{x} \sim \mathbb{D}, \mathcal{T}_{1,2} \sim \mathbb{T}} \ell(f_\theta(\mathcal{T}_1(\mathbf{x})), f_\theta(\mathcal{T}_2(\mathbf{x}))). \quad (1)$$

where $\ell(\cdot, \cdot)$ is a loss function. In particular, the Siamese network usually consists of an encoder $E_{\theta_e}(\cdot)$ and a projector $G_{\theta_g}(\cdot)$. Their outputs $\mathbf{h} = E_{\theta_e}(\mathcal{T}(\mathbf{x}))$ and $\mathbf{z} = G_{\theta_g}(\mathbf{h})$ are referred to as *encoding* and *embedding*, respectively. We summarize the notations and use the corresponding capital letters denoting mini-batch data in Figure 1. Under this notation, we have $f_\theta(\cdot) = G_{\theta_g}(E_{\theta_e}(\cdot))$ with learnable parameters $\theta = \{\theta_e, \theta_g\}$. The *encoding* \mathbf{h} is usually used as representation for evaluation by either training a linear classifier [21] or transferring to downstream tasks. This is due to that \mathbf{h} is shown to obtain significantly better performance than the *embedding* \mathbf{z} [6, 8].

The mean square error (MSE) of L_2 -normalized vectors is usually used as the loss function [8]:

$$\ell(\mathbf{z}_1, \mathbf{z}_2) = \left\| \frac{\mathbf{z}_1}{\|\mathbf{z}_1\|_2} - \frac{\mathbf{z}_2}{\|\mathbf{z}_2\|_2} \right\|_2^2, \quad (2)$$

where $\|\cdot\|_2$ denotes the L_2 norm. This loss is also equivalent to the negative cosine similarity, up to a scale of $\frac{1}{2}$ and an optimization irrelevant constant.

Collapse and Whitening Loss. While minimizing Eqn. 1, a trivial solution known as *collapse* could occur such that $f_\theta(\mathbf{x}) \equiv \mathbf{c}$, $\forall \mathbf{x} \in \mathbb{D}$. The state of *collapse* will provide no gradients for learning and offer no information for discrimination. Moreover, a weaker collapse condition called *dimensional collapse* can be easily arrived, for which the projected features collapse into a low-dimensional manifold. As illustrated in [24], dimensional collapse is associated with strong correlations between axes, which motivates the use of whitening method in avoiding the dimensional collapse. The general idea of whitening loss [13] is to minimize Eqn. 1, under the condition that *embeddings* from different views are whitened, which can be formulated as³:

$$\begin{aligned} \min_{\theta} \mathcal{L}(\mathbf{x}; \theta) &= \mathbb{E}_{\mathbf{x} \sim \mathbb{D}, \mathcal{T}_{1,2} \sim \mathbb{T}} \ell(\mathbf{z}_1, \mathbf{z}_2), \\ \text{s.t. } \text{cov}(\mathbf{z}_i, \mathbf{z}_i) &= \mathbf{I}, i \in \{1, 2\}. \end{aligned} \quad (3)$$

Whitening loss provides theoretical guarantee in avoiding (dimensional) collapse, since the embedding is whitened with all axes decorrelated [13, 24]. While it is difficult to directly solve the problem of Eqn. 3, Ermolov *et al.* [13] propose to whiten the mini-batch embedding $\mathbf{Z} \in \mathbb{R}^{d_z \times m}$ using batch whitening (BW) [25, 41] and impose the loss on the whitened output $\widehat{\mathbf{Z}} \in \mathbb{R}^{d_z \times m}$, given the mini-batch inputs \mathbf{X} with size of m , as follows:

$$\begin{aligned} \min_{\theta} \mathcal{L}(\mathbf{X}; \theta) &= \mathbb{E}_{\mathbf{X} \sim \mathbb{D}, \mathcal{T}_{1,2} \sim \mathbb{T}} \|\widehat{\mathbf{Z}}_1 - \widehat{\mathbf{Z}}_2\|_F^2 \\ \text{with } \widehat{\mathbf{Z}}_i &= \Phi(\mathbf{Z}_i), i \in \{1, 2\}, \end{aligned} \quad (4)$$

where $\Phi(\cdot)$ denotes the whitening transformation over mini-batch data.

³The dual view formulation can be extended to s different views, as shown in [13].

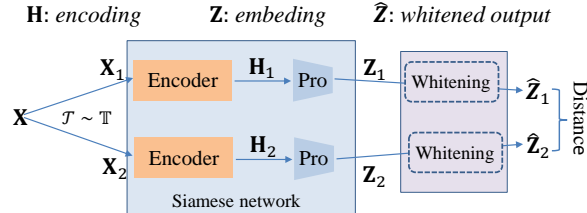


Figure 1: The basic notations for SSL used in this paper.

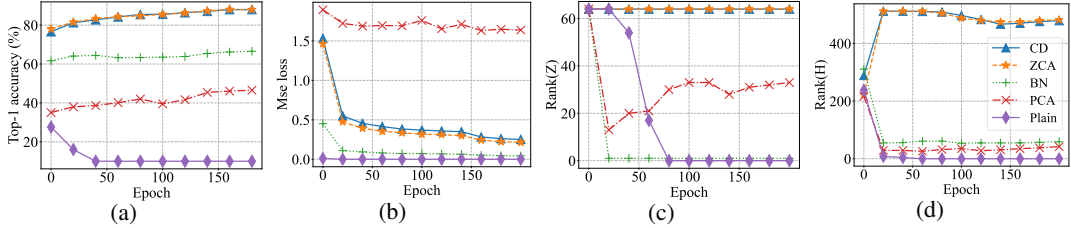


Figure 2: Effects of different whitening transformations for SSL. We use the ResNet-18 as the encoder (dimension of representation is 512.), a two layer MLP with ReLU and BN appended as the projector (dimension of embedding is 64). The model is trained on CIFAR-10 for 200 epochs with batch size of 256 and standard data argumentation, using Adam optimizer [30] (more details of experimental setup please see [Appendix A.2](#)). We show (a) the linear evaluation accuracy; (b) the training loss; (c) the rank of *embedding*; (d) the rank of *encoding*.

Whitening Transformations. There are an infinite number of possible whitening matrices, as shown in [29, 25], since any whitened data with a rotation is still whitened. For simplifying notation, we assume \mathbf{Z} is centered by $\mathbf{Z} := \mathbf{Z}(\mathbf{I} - \frac{1}{m}\mathbf{1}\mathbf{1}^T)$. Ermolov *et al.* [13] propose W-MSE that uses Cholesky decomposition (CD) whitening: $\Phi_{CD}(\mathbf{Z}) = \mathbf{L}^{-1}\mathbf{Z}$ in Eqn. 4, where \mathbf{L} is a lower triangular matrix from the Cholesky decomposition, with $\mathbf{L}\mathbf{L}^T = \Sigma$. Here $\Sigma = \frac{1}{m}\mathbf{Z}\mathbf{Z}^T$ is the covariance matrix of the *embedding*. Hua *et al.* [24] use zero-phase component analysis (ZCA) whitening [25] in Eqn. 4: $\Phi_{ZCA} = \mathbf{U}\Lambda^{-\frac{1}{2}}\mathbf{U}^T$, where $\Lambda = \text{diag}(\lambda_1, \dots, \lambda_{d_z})$ and $\mathbf{U} = [\mathbf{u}_1, \dots, \mathbf{u}_{d_z}]$ are the eigenvalues and associated eigenvectors of Σ , *i.e.*, $\mathbf{U}\Lambda\mathbf{U}^T = \Sigma$. Another famous whitening is principal components analysis (PCA) whitening: $\Phi_{PCA} = \Lambda^{-\frac{1}{2}}\mathbf{U}^T$ [29, 25].

3.2 Empirical Investigation on Whitening Loss

In this section, we conduct experiments to investigate the effects of different whitening transformations $\Phi(\cdot)$ used in Eqn. 4 for SSL. Besides, we investigate the performances of different features (including *encoding* \mathbf{H} , *embedding* \mathbf{Z} and the whitened output $\widehat{\mathbf{Z}}$) used as representation for evaluation. For illustration, we first define the *rank* and *stable-rank* [46] of a matrix as follows:

Definition 1. Given a matrix $\mathbf{A} \in \mathbb{R}^{d \times m}$, $d \leq m$, we denote $\{\lambda_1, \dots, \lambda_d\}$ the singular values of \mathbf{A} in a descent order with convention $\lambda_1 > 0$. The **rank** of \mathbf{A} is the number of its non-zero singular values, denoted as $\text{Rank}(\mathbf{A}) = \sum_{i=1}^d \mathbb{I}(\lambda_i > 0)$, where $\mathbb{I}(\cdot)$ is the indicator function. The **stable-rank** of \mathbf{A} is denoted as $r(\mathbf{A}) = \frac{\sum_{i=1}^d \lambda_i}{\lambda_1}$.

By definition, $\text{Rank}(\mathbf{A})$ can be a good indicator to evaluate the extent of *dimensional collapse* of \mathbf{A} , and $r(\mathbf{A})$ can be an indicator to evaluate the extent of whitening of \mathbf{A} . It can be demonstrated that $r(\mathbf{A}) \leq \text{Rank}(\mathbf{A}) \leq d$ [46]. Note that if \mathbf{A} is fully whitened with covariance matrix $\mathbf{A}\mathbf{A}^T = m\mathbf{I}$, we have $r(\mathbf{A}) = \text{Rank}(\mathbf{A}) = d$. We also define normalized rank as $\widehat{\text{Rank}}(\mathbf{A}) = \frac{\text{Rank}(\mathbf{A})}{d}$ and normalized stable-rank as $\widehat{r}(\mathbf{A}) = \frac{r(\mathbf{A})}{d}$, for comparing the extent of *dimensional collapse* and whitening of matrices with different dimensions, respectively.

PCA Whitening Fails to Avoid Dimensional Collapse. We compare the effects of ZCA, CD, PCA transformations for whitening loss, evaluated on CIFAR-10 using the standard setup for SSL (see Section 4.1 for details). Besides, we also provide the result of batch normalization (BN) that only performs standardization without decorrelating the axes, and the ‘Plain’ method that imposes the loss directly on *embedding*. From Figure 2, we observe that naively training a Siamese network (‘Plain’) results in collapse both on the *embedding* (Figure 2(c)) and *encoding* (Figure 2(d)), which significantly hampers the performance (Figure 2(a)), although its training loss becomes close to zero (Figure 2(b)). We also observe that an extra BN imposed on the *embedding* prevents collapse to a point. However, it suffers from the dimensional collapse where the rank of *embedding* and *encoding* are significantly low, which also hampers the performance. ZCA and CD whitening both maintain high rank of *embedding* and *encoding* by decorrelating the axes, ensuring high linear evaluation accuracy. However, we note that PCA whitening shows significantly different behaviors: PCA whitening cannot decrease the loss and even cannot avoid the dimensional collapse, which also leads to significantly downgraded performance. This interesting observation challenges the motivations of whitening loss for SSL. We defer the analyses and illustration in Section 3.3.

Whitened Output is not a Good Representation. As introduced before, the motivation of whitening loss for SSL is that the whitening operation can remove the correlation among axes [24] and a

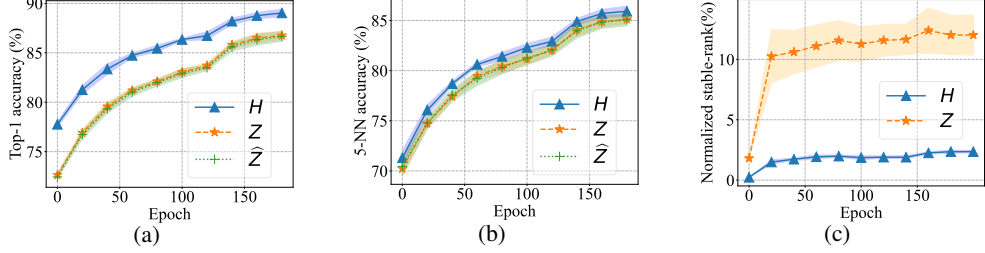


Figure 3: Comparisons of features when using *encoding* \mathbf{H} , *embedding* \mathbf{Z} and whitened output $\hat{\mathbf{Z}}$ respectively. We follow the same experimental setup as Figure 2. We show (a) the linear evaluation accuracy; (b) the kNN accuracy; (c) the normalized stable-rank for comparing the extent of whitening (note that the normalized stable-rank of $\hat{\mathbf{Z}}$ is always 100% during training and we omit it for clarity). The results are averaged by five random seeds, with standard deviation shown using shaded region.

whitened representation ensures that the examples scattered in a spherical distribution [13], which is sufficient to avoid collapse. Based on this argument, one should use the whitened output $\hat{\mathbf{Z}}$ as the representation for downstream tasks, rather than the *encoding* \mathbf{H} that is commonly used. This raises questions that whether \mathbf{H} is well whitened and whether the whitened output is a good feature. We conduct experiments to compare the performances of whitening loss, when using \mathbf{H} , \mathbf{Z} and $\hat{\mathbf{Z}}$ as representations for evaluation respectively. The results are shown in Figure 3. We observe that using whitened output $\hat{\mathbf{Z}}$ as a representation has significantly worse performance than using \mathbf{H} . Furthermore, we find that the normalized stable rank of \mathbf{H} is significantly smaller than 100%, which suggests that \mathbf{H} is not well whitened. These results show that the whitened output could not be a good representation.

3.3 Analysing Decomposition of Whitening Loss

For clarity, we use the mini-batch input with size of m . Given one mini-batch input \mathbf{X} with two augmented views, Eqn. 4 can be formulated as:

$$\mathcal{L}(\mathbf{X}) = \frac{1}{m} \|\hat{\mathbf{Z}}_1 - \hat{\mathbf{Z}}_2\|_F^2. \quad (5)$$

Let us consider a proxy loss described as:

$$\mathcal{L}'(\mathbf{X}) = \underbrace{\frac{1}{m} \|\hat{\mathbf{Z}}_1 - (\hat{\mathbf{Z}}_2)_{st}\|_F^2}_{\mathcal{L}'_1} + \underbrace{\frac{1}{m} \|(\hat{\mathbf{Z}}_1)_{st} - \hat{\mathbf{Z}}_2\|_F^2}_{\mathcal{L}'_2}, \quad (6)$$

where $(\cdot)_{st}$ indicates the stop-gradient operation. It is easy to demonstrate that $\frac{\partial \mathcal{L}}{\partial \theta} = \frac{\partial \mathcal{L}'}{\partial \theta}$ (see [Appendix B.1](#) for proof). That is, the optimization dynamics of \mathcal{L} is equivalent to \mathcal{L}' . By looking into the first term of Eqn. 14, we have:

$$\mathcal{L}'_1 = \frac{1}{m} \|\phi(\mathbf{Z}_1)\mathbf{Z}_1 - (\hat{\mathbf{Z}}_2)_{st}\|_F^2. \quad (7)$$

Here, we can view $\phi(\mathbf{Z}_1)$ as a predictor that depends on \mathbf{Z}_1 during forward propagation, and $\hat{\mathbf{Z}}_2$ as a whitened target with $r(\hat{\mathbf{Z}}_2) = \text{Rank}(\hat{\mathbf{Z}}_2) = d_z$. In this way, we find that minimizing \mathcal{L}'_1 only requires the embedding \mathbf{Z}_1 being full-rank with $\text{Rank}(\hat{\mathbf{Z}}_1) = d_z$, as stated by following proposition.

Proposition 1. *Let $\mathbb{A} = \arg \min_{\mathbf{Z}_1} \mathcal{L}'_1(\mathbf{Z}_1)$. We have that \mathbb{A} is not an empty set, and $\forall \mathbf{Z}_1 \in \mathbb{A}$, \mathbf{Z}_1 is full-rank. Furthermore, for any $\{\sigma_i\}_{i=1}^{d_z}$ with $\sigma_1 \geq \sigma_2 \geq \dots, \sigma_{d_z} > 0$, we construct $\tilde{\mathbb{A}} = \{\mathbf{Z}_1 | \mathbf{Z}_1 = \mathbf{U}_2 \text{diag}(\sigma_1, \sigma_2, \dots, \sigma_{d_z}) \mathbf{V}_2^T, \text{where } \mathbf{U}_2 \in \mathbb{R}^{d_z \times d_z} \text{ and } \mathbf{V}_2 \in \mathbb{R}^{m \times d_z} \text{ are from the singular value decomposition of } \hat{\mathbf{Z}}_2$, i.e., $\mathbf{U}_2(\sqrt{m}\mathbf{I})\mathbf{V}_2^T = \hat{\mathbf{Z}}_2$. When we use ZCA whitening, we have $\tilde{\mathbb{A}} \subseteq \mathbb{A}$.*

The proof is shown in [Appendix B.2](#). Proposition 1 states that there are infinity matrix with full-rank that is the optimum when minimizing \mathcal{L}'_1 w.r.t. \mathbf{Z}_1 . Therefore, minimizing \mathcal{L}'_1 only requires the embedding \mathbf{Z}_1 being full-rank with $\text{Rank}(\hat{\mathbf{Z}}_1) = d_z$, and does not necessarily impose the constraints on \mathbf{Z}_1 to be whitened with $r(\mathbf{Z}_1) = d_z$. Similar analysis also applies to \mathcal{L}'_2 and minimizing \mathcal{L}'_2

requires \mathbf{Z}_2 being full-rank. Therefore, BW-based methods shown in Eqn. 4 do not impose whitening constraints on the embedding as formulated in Eqn. 3, but they only require the embedding to be **full-rank**. This full-rank constraint is also sufficient to avoid dimensional collapse for embedding, even though it is a weaker constraint than whitening.

Our analysis further implies that whitening loss in its symmetric formulation (Eqn. 5) can be decomposed into two asymmetric losses (Eqn. 14), where each asymmetric loss requires an online network to match a whitened target. This mechanism provides a pivot connecting to other methods, and a clue to understand why PCA whitening fails to avoid dimensional collapse for SSL.

Connection to Asymmetric Methods. The asymmetric formulation of whitening loss shown in Eqn. 7 bears resemblance to those asymmetry methods without negative pairs, *e.g.*, SimSiam [8]. In these methods, an extra predictor is incorporated and the stop-gradient is essential for avoid collapse. In particular, SimSiam uses the objective as:

$$\mathcal{L}(\mathbf{X}) = \frac{1}{m} \|P_{\theta_p}(\cdot) \circ \mathbf{Z}_1 - (\mathbf{Z}_2)_{st}\|_F^2 + \frac{1}{m} \|P_{\theta_p}(\cdot) \circ \mathbf{Z}_2 - (\mathbf{Z}_1)_{st}\|_F^2, \quad (8)$$

where $P_{\theta_p}(\cdot)$ is the predictor with learnable parameters θ_p . By contrasting Eqn. 7 and the first term of Eqn. 8, we find that: 1) BW-based whitening loss ensures a whitened target $\widehat{\mathbf{Z}}_2$, while SimSiam does not put constraint on the target \mathbf{Z}_2 ; 2) SimSiam uses a learnable predictor $P_{\theta_p}(\cdot)$, which is shown to empirically avoid collapse by matching the rank of the covariance matrix by back-propagation [44], while BW-based whitening loss has an implicit predictor $\phi(\mathbf{Z}_1)$ depending on the input itself, which is a full-rank matrix by design. Based on this analysis, we find that BW-based whitening loss can surely avoid collapse if the loss converges well, while SimSiam can not provide such a guarantee in avoiding collapse. Similar analysis also applies to BYOL [18], except that BYOL uses a momentum target network for providing target signal.

Connection to Soft Whitening. VICReg [2] also encourages whitened *embedding* produced from different views, but by imposing a whitening penalty as a regularization on the *embedding*, which is called soft whitening. In particular, given a mini-batch input, the objective of VICReg is as follows⁴:

$$\mathcal{L}(\mathbf{X}) = \frac{1}{m} \|\mathbf{Z}_1 - \mathbf{Z}_2\|_F^2 + \alpha \sum_{i=1}^2 \left(\left\| \frac{1}{m} \mathbf{Z}_i \mathbf{Z}_i^T - \lambda \mathbf{I} \right\|_F^2 \right), \quad (9)$$

where $\alpha \geq 0$ is the penalty factor. Similarly, we can use a proxy loss for VICReg and considering its term corresponding to optimizing \mathbf{Z}_1 only (similar to Eqn. 7), we have:

$$\mathcal{L}'_{VICReg}(\mathbf{X}) = \frac{1}{m} \|\mathbf{Z}_1 - (\mathbf{Z}_2)_{st}\|_F^2 + \alpha \left\| \frac{1}{m} \mathbf{Z}_1 \mathbf{Z}_1^T - \lambda \mathbf{I} \right\|_F^2. \quad (10)$$

Based on this formulation, we observe that VICReg requires *embedding* \mathbf{Z}_1 to be whitened by, 1) the additional whitening penalty, and 2) fitting the (expected) whitened targets \mathbf{Z}_2 . By contrasting Eqns. 7 and 10, we highlight that the so-called hard whitening methods, like W-MSE [13], only impose full-rank constraints on the embedding, while soft whitening methods indeed impose whitening constraints. Similar analysis also applies to Barlow Twins [49], except that the whitening/decorrelation penalty is imposed on the cross-covariance matrix of embedding from different views.

Connection to Other Non-contrastive Methods. SwAV [4], a clustering-based method, uses a "swapped" prediction mechanism where the cluster assignment (code) of a view is predicted from the representation of another view, by minimizing the following objective:

$$\mathcal{L}(\mathbf{X}) = \ell(\mathbf{C}^T \mathbf{Z}_1, (\mathbf{Q}_2)_{st}) + \ell(\mathbf{C}^T \mathbf{Z}_2, (\mathbf{Q}_1)_{st}). \quad (11)$$

Here, \mathbf{C} is the prototype matrix learned by back-propagation, \mathbf{Q}_i is the predicted code with equal-partition and high-entropy constraints, and SwAV uses cross-entropy loss as $\ell(\cdot, \cdot)$ to match the distributions. The constraints on \mathbf{Q}_i are approximately satisfied during optimization, by using the iterative Sinkhorn-Knopp algorithm conditioned on the input $\mathbf{C}^T \mathbf{Z}_i$. Note that SwAV explicitly uses stop-gradient when it calculates the target \mathbf{Q}_i . By contrasting Eqn. 7 and the first term of Eqn. 11, we find that: 1) SwAV can be viewed as an online network to match a target with constraints, like BW-based whitening loss, even though the constraints imposed on the targets between them are

⁴Note the slight difference where VICReg uses margin loss on the diagonal of covariance, while our notation uses MSE loss.

different; 2) From the perspective of asymmetric structure, SwAV indeed uses a linear predictor \mathbf{C}^T that is also learned by back-propagation like SimSiam, while BW-based whitening loss has an implicit predictor $\phi(\mathbf{Z}_1)$ depending on the input itself. Similar analysis also applies to DINO [5], which further simplifies the formulation of SwAV by removing the prototype matrix and directly matching the output of another view, from the view of knowledge distillation. DINO uses centering and sharpening operations to impose the constraints on the target (output of another view). One significant difference between DINO and whitening loss is that DINO uses population statistics of centering calculated by moving average, while whitening loss uses the mini-batch statistics of whitening.

Why PCA Whitening Fails to Avoid Dimensional Collapse? Based on Eqn. 7, we note that whitening loss can favorably provide full-rank constraints on the embedding under the condition that the online network can match the whitened targets well. We experimentally find that PCA-based whitening loss provides volatile sequence of whitened targets during training, as shown in Figure 4(a). It is difficult for the online network to match such a target signal with significant variation, resulting in minimal decrease in the whitening loss (see Figure 2). Furthermore, we observe that PCA-based whitening loss has also significantly varying whitening matrix sequences $\{\phi^t(\cdot)\}$ (Figure 4(b)), even given the same input data. This coincides with the observation in [18, 8], where an unstable predictor results in significant degenerate performance. Our observations are also in accordance with the arguments in [25, 26] that PCA-based BW shows significantly large stochasticity. We note that ZCA whitening can provide relatively stable sequences of whitened targets and whitening matrix during training (Figure 4), which ensures stable training for SSL. This is likely due to the property of ZCA-based whitening that minimizes the total squared distance between the original and whitened variables [29, 25].

Why Whitened Output is not a Good Representation? A whitened output removes the correlation among axes [24] and ensures the examples scattered in a spherical distribution [13], which bears resemblance to contrastive learning where different examples are pulled away. We conduct experiments to compare SimCLR [6], BYOL [18], VICReg [2] and W-MSE [13], and monitor the cosine similarity for all negative pairs, stable-rank and rank during training. From Figure 5, we find that all methods can achieve a high rank on the *encoding*. This is driven by the improved extent of whitening on the *embedding*. Furthermore, we observe that the negatives cosine similarity decreases during the training, while the extent of stable-rank increases, for all methods. This observation suggests that a representation with stronger extent of whitening is more likely to have less similarity among different examples. We further conduct experiments to validate this argument, using VICReg

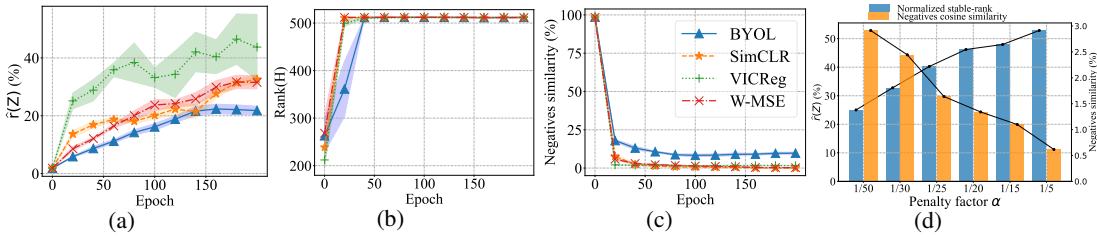


Figure 5: Comparison of different SSL methods. We follow the same experimental setup as Figure 2. We show (a) the normalized stable-rank of *embedding*; (b) the rank of *encoding*; (c) the negatives cosine similarity, calculated on the *embeddings* from all negative pairs (different examples). We also train VICReg with varying penalty factor α to show the relationship between the normalized stable-rank and negatives cosine similarity in (d). Here, we use embedding dimension of 64. We have similar observations when using the embedding dimension of other numbers (e.g., 128 and 256).

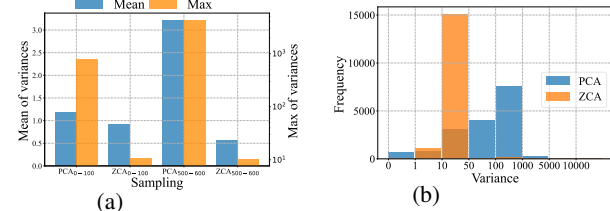


Figure 4: Illustration of PCA-based whitening loss suffering from training instability. We follow the same experimental setup as Figure 2. Given a certain mini-batch input ($m = 2048$), we monitor its whitened output $\widehat{\mathbf{Z}}^t$ and whitening matrix Φ^t for each epoch t . We calculate the variance along the training epochs for each element of $\widehat{\mathbf{Z}}$ and Φ . We show (a) the mean and maximum of variances of $\widehat{\mathbf{Z}}$, noting that PCA_{0-100} indicates the variance of PCA whitened output is calculated along the first 100 epochs; and (b) the histogram of variance of Φ .

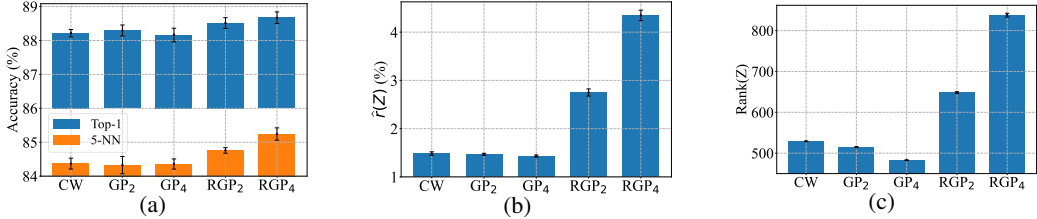


Figure 6: Illustration of CW with random group partition. We follow the same experimental setup as Figure 2, except that we set the dimension of embedding as 2048 tailored for CW. We use ‘GP₂’ (‘RGP₂’) to indicate CW using group partition (random group partition), with a group number of 2. (a) The linear and k-NN accuracies; (b) The normalized stable-rank of embedding; (c) The rank of embedding. All experiments are repeated five times, with standard deviation shown as error bars.

with varying penalty factor α (Eqn. 10) to adjust the extent of whitening on *embedding* (Figure 5(d)). Therefore, a whitened output leads to the state that all examples have dissimilar features. This state can break the potential manifold the examples in the same class belong to, which makes the learning more difficult [19]. Similar analysis for contrastive learning is also shown in [6], where classes represented by the projected output (*embedding*) are not well separated, compared to *encoding*.

4 Channel Whitening with Random Group Partition

One main weakness of BW-based whitening loss is that the whitening operation requires the number of examples (mini-batch size) m to be larger than the size of channels d , to avoid numerical instability⁵. This requirement limits its usage in scenarios where large batch of training data cannot be fit into the memory. Based on previous analysis, the whitening loss can be viewed as an online learner to match a whitened target with all singular values being one. We note the key of whitening loss is that it conducts a transformation $\phi : \mathbf{Z} \rightarrow \widehat{\mathbf{Z}}$, ensuring that the singular values of $\widehat{\mathbf{Z}}$ are one. We thus propose channel whitening (CW) that ensures the examples in a mini-batch are orthogonal:

$$\text{Centering} : \mathbf{Z}_c = (\mathbf{I} - \frac{1}{d}\mathbf{1}\cdot\mathbf{1}^T)\mathbf{Z}, \quad \text{Whitening} : \widehat{\mathbf{Z}} = \mathbf{Z}_c\Phi, \quad (12)$$

where $\Phi \in \mathbb{R}^{m \times m}$ is the ‘whitening matrix’ that is derived from the corresponding ‘covariance matrix’: $\Sigma' = \frac{1}{d-1}\mathbf{Z}_c^T\mathbf{Z}_c$. In our implementation, we use ZCA whitening to obtain Φ . CW ensures the examples in a mini-batch are orthogonal to each other, with $\widehat{\mathbf{Z}}^T\widehat{\mathbf{Z}} = \frac{1}{d-1}\mathbf{I}$. This means CW has the same ability as BW for SSL in avoiding the dimensional collapse, by providing target $\widehat{\mathbf{Z}}$ whose singular values are one. More importantly, one significant advantage of CW is that it can obtain numerical stability when the batch size is small, since the condition that $d > m$ can be obtained by design (*e.g.*, we can set the channel number of embedding d to be larger than the batch size m). Besides, we find that CW can amplify the full-rank constraints on the embedding by dividing the channels/neurons into random groups, as we will illustrate.

Random Group Partition. Given the embedding $\mathbf{Z} \in \mathbb{R}^{d \times m}, d > m$, we divide it into $g \geq 1$ groups $\{\mathbf{Z}^{(i)} \in \mathbb{R}^{\frac{d}{g} \times m}\}_{i=1}^g$, where we assume that d is divisible by g and ensure $\frac{d}{g} > m$. We then perform CW on each $\mathbf{Z}^{(i)}, i = 1, \dots, g$. Note that the ranks of \mathbf{Z} and $\mathbf{Z}^{(i)}$ are all at most m . Therefore, CW with group partition provides g constraints with $\text{Rank}(\mathbf{Z}^{(i)}) = m$ on embedding, compared to CW without group partition that only one constraint with $\text{Rank}(\mathbf{Z}) = m$. Although CW with group partition can provide more full-rank constraints for mini-batch data, we find that it can also make the population data correlated, if group partition is all the same during training, which decreases the rank and does not improve the performance in accuracy by our experiments (Figure 6). We find random group partition, which randomly divide the channels/neurons into group for each iteration (mini-batch data), can alleviate this issue and obtain an improved performance, from Figure 6. We call our method as channel whitening with random group partition (CW-RGP), and provide the full algorithm and PyTorch-style code in [Appendix C](#).

We note that Hua *et al.* [24] use a similar idea for BW, called Shuffled-DBN. However Shuffled-DBN cannot well amplify the full-rank constraints by using more groups, since BW-based methods require $m > \frac{d}{g}$ to avoid numerical instability. We further show that CW-RGP works remarkably better than

⁵An empirical setting is $m = 2d$ that can obtain good performance as shown in [13, 24].

Table 1: Classification accuracy (top 1) of a linear classifier and a 5-nearest neighbors classifier for different loss functions and datasets with a ResNet-18 encoder.

Method	CIFAR-10		CIFAR-100		STL-10		Tiny-ImageNet	
	linear	5-nn	linear	5-nn	linear	5-nn	linear	5-nn
SimCLR [6]	91.80	88.42	66.83	56.56	90.51	85.68	48.84	32.86
BYOL [18]	91.73	89.45	66.60	56.82	91.99	88.64	51.00	36.24
SimSiam [8] (repro.)	90.51	86.82	66.04	55.79	88.91	84.84	48.29	34.21
Shuffled-DBN [24] (repro.)	90.45	88.15	66.07	56.97	89.20	84.51	48.60	32.14
Barlow Twins [49] (repro.)	88.51	86.53	65.78	55.76	88.36	83.71	47.44	32.65
VICReg [2] (repro.)	90.32	88.41	66.45	56.78	90.78	85.72	48.71	33.35
Zero-ICL [52] (repro.)	88.12	86.64	61.91	53.47	86.35	82.51	46.25	32.74
W-MSE 2 [13]	91.55	89.69	66.10	56.69	90.36	87.10	48.20	34.16
W-MSE 4 [13]	91.99	89.87	67.64	56.45	91.75	88.59	49.22	35.44
CW-RGP 2 (ours)	91.92	89.54	67.51	57.35	90.76	87.34	49.23	34.04
CW-RGP 4 (ours)	92.47	90.74	68.26	58.67	92.04	88.95	50.24	35.99

Shuffled-DBN in the subsequent experiments. We attribute this results to the ability of CW-RGP in amplifying the full-rank constraints by using groups.

4.1 Experiments for Empirical Study

In this section, we conduct experiments to validate the effectiveness of our proposed CW-RGP. We evaluate the performances of CW-RGP for classification on CIFAR-10, CIFAR-100 [31], STL-10 [10], TinyImageNet [32] and ImageNet [12]. We also evaluate the effectiveness in transfer learning, for a pre-trained model using CW-RGP. We run the experiments on one workstation with 4 GPUs. For more details of implementation and training protocol, please refer to [Appendix A.3](#) and D.

Evaluation for Classification We first conduct experiments on small and medium size datasets (including CIFAR-10, CIFAR-100, STL-10 and Tiny-ImageNet), strictly following the setup of W-MSE paper [13]. Our CW-RGP inherits the advantages of W-MSE in exploiting different views. CW-RGP 2 and CW-RGP 4 indicate our methods with $s = 2$ and $s = 4$ positive views extracted per image respectively, similar to W-MSE [13]. The results of baselines shown in Table. 1 are partly inherited in [13], except that we reproduce certain baselines under the same training and evaluation settings as in [13] (some different hyper-parameter settings are shown in [Appendix A.3](#)). We observe that CW-RGP obtains the highest accuracy on almost all the datasets except Tiny-ImageNet. Besides, CW-RGP with 4 views are generally better than 2, similar to W-MSE. These results show that CW-RGP is a competitive SSL method. We also confirm that CW with random group partition could obtain a higher performance than BW (and with random group partition), comparing CW-RGP to W-MSE and Shuffled-DBN.

We then conduct experiments on large-scale ImageNet, strictly following the setup of SimSiam paper [8]. The results of baselines shown in Table 2 are mostly reported in [8], except that the result of W-MSE 4 is from the W-MSE paper [13] and we reproduce BYOL [18], SwAV [4] and W-MSE 4 [13] under a batch size of 512 based on the same training and evaluation settings as in [8] for fairness. CW-RGP 4 is trained with a batch size of 512 and gets the highest accuracy among all methods under both 100 and 200 epochs training. We find that our CW-RGP can also work well when combined with the whitening penalty used in VICReg. Note that we also try a batch size of 256 under 100-epoch training, which gets the top-1 accuracy of 69.5%.

Transfer to downstream tasks We examine the representation quality by transferring our model to other tasks, including VOC [14] object detection, COCO [35] object detection and instance segmentation. We use the baseline (except for the pre-training model, the others are exactly the same) of the detection codebase from MoCo [21] for CW-RGP to produce the results. The results of baselines shown in Table3 are mostly inherited from [8]. We clearly observe that CW-RGP performs better than or on par with these state-of-the-art approaches on COCO object detection and instance segmentation, which shows the great potential of CW-RGP in transferring to downstream tasks.

Table 2: Comparisons on ImageNet linear classification. All are based on ResNet-50 encoder. The table is mostly inherited from [8].

Method	Batch size	100 eps	200 eps
SimCLR [6]	4096	66.5	68.3
MoCo v2 [7]	256	67.4	69.9
BYOL [18]	4096	66.5	70.6
SwAV [4]	4096	66.5	69.1
SimSiam [8]	256	68.1	70.0
W-MSE 4 [13]	4096	69.4	-
Zero-CL [52]	1024	68.9	-
BYOL [18] (repro.)	512	66.1	69.2
SwAV [4] (repro.)	512	65.8	67.9
W-MSE 4 [13] (repro.)	512	66.7	67.9
CW-RGP 4 (ours)	512	69.7	71.0

Table 3: Transfer Learning. All competitive unsupervised methods are based on 200-epoch pre-training in ImageNet (IN). The table is mostly inherited from [8]. Our CW-RGP is performed with 3 random seeds, with mean and standard deviation reported.

Method	VOC 07+12 detection			COCO detection			COCO instance seg.		
	AP ₅₀	AP	AP ₇₅	AP ₅₀	AP	AP ₇₅	AP ₅₀	AP	AP ₇₅
Scratch	60.2	33.8	33.1	44.0	26.4	27.8	46.9	29.3	30.8
IN-supervised	81.3	53.5	58.8	58.2	38.2	41.2	54.7	33.3	35.2
SimCLR [6]	81.8	55.5	61.4	57.7	37.9	40.9	54.6	33.3	35.3
MoCo v2 [7]	82.3	57.0	63.3	58.8	39.2	42.5	55.5	34.3	36.6
BYOL [18]	81.4	55.3	61.1	57.8	37.9	40.9	54.3	33.2	35.0
SwAV [4]	81.5	55.4	61.4	57.6	37.6	40.3	54.2	33.1	35.1
SimSiam [8]	82.0	56.4	62.8	57.5	37.9	40.9	54.2	33.2	35.2
CW-RGP (ours)	82.2_{±0.07}	57.2_{±0.10}	63.8_{±0.11}	60.5_{±0.28}	40.7_{±0.14}	44.1_{±0.14}	57.3_{±0.16}	35.5_{±0.12}	37.9_{±0.14}

Ablation for Random Group Partition. We also conduct experiments to show the advantages of random group partition for channel whitening. We use ‘CW’, ‘CW-GP’ and ‘CW-RGP’ to indicate channel whitening without group partition, with group partition and with random group partition, respectively. We further consider the setup with $s = 2$ and $s = 4$ positive views. We use the same setup as in Table 1 and show the results in Table 4. We have similar observation as in Figure 6 that CW with random group partition improves the performance.

Ablation for Batch Size. Here, we conduct experiments to empirically show the advantages of CW over BW, in terms of the stability using different batch size. We train CW and BW on ImageNet-100, using batch size ranging in $\{32, 64, 128, 256\}$. Figure 7 shows the results. We can find that CW is more robust for small batch size training.

5 Conclusion and Limitation

In this paper, we invested whitening loss for SSL, and observed several interesting phenomena with further clarification based on our analysis framework. We showed that batch whitening (BW) based methods only require the embedding to be full-rank, which is also a sufficient condition for collapse avoidance. We proposed channel whitening with random group partition (CW-RGP) that is well motivated theoretically in avoiding a collapse and has been validated empirically in learning good representation.

Limitation. Our work only shows how to avoid collapse by using whitening loss, but does not explicitly show what should be the extent of whitening of a good representation. We note that a concurrent work addresses this problem by connecting the eigenspectrum of a representation to a power law [17], and shows the coefficient of the power law is a strong indicator for the effects of representation. We believe our work can be further extended when combined with the analyses from [17]. Besides, our work does not answer how the projector affects the extents of whitening between *encoding* and *embedding* [20], which is important to answer why *encoding* is usually used as a representation for evaluation, rather than the whitened output or *embedding*. Our attempts, shown in [Appendix E](#), provide preliminary results, but does not offer an answer to this question.

Acknowledgement This work was partially supported by the National Key Research and Development Plan of China under Grant 2021ZD0112901, National Natural Science Foundation of China (Grant No. 62106012), the Fundamental Research Funds for the Central Universities.

Table 4: Results of ablation for random group partition.

Method	CIFAR-10		CIFAR-100	
	linear	5-nn	linear	5-nn
CW 2	91.66	88.99	66.26	56.36
CW-GP 2	91.61	88.89	66.17	56.53
CW-RGP 2	91.92	89.54	67.51	57.35
CW 4	92.10	90.12	66.90	57.12
CW-GP 4	92.08	90.06	67.34	57.28
CW-RGP 4	92.47	90.74	68.26	58.67

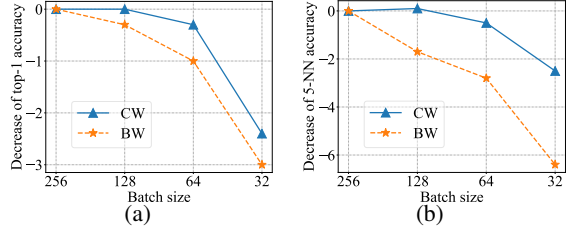


Figure 7: Decrease in top-1 and 5-nn accuracy (in % points) of CW and BW at 100 epochs on ImageNet-100.

References

- [1] Bachman, P., Hjelm, R.D., Buchwalter, W.: Learning representations by maximizing mutual information across views. In: NeurIPS (2019)
- [2] Bardes, A., Ponce, J., LeCun, Y.: Vicreg: Variance-invariance-covariance regularization for self-supervised learning. In: ICLR (2022)
- [3] Caron, M., Bojanowski, P., Joulin, A., Douze, M.: Deep clustering for unsupervised learning of visual features. In: ECCV (2018)
- [4] Caron, M., Misra, I., Mairal, J., Goyal, P., Bojanowski, P., Joulin, A.: Unsupervised learning of visual features by contrasting cluster assignments. In: NeurIPS (2020)
- [5] Caron, M., Touvron, H., Misra, I., Jegou, H., Mairal, J., Bojanowski, P., Joulin, A.: Emerging properties in self-supervised vision transformers. In: ICCV (2021)
- [6] Chen, T., Kornblith, S., Norouzi, M., Hinton, G.: A simple framework for contrastive learning of visual representations. In: ICML (2020)
- [7] Chen, X., Fan, H., Girshick, R., He, K.: Improved baselines with momentum contrastive learning. arXiv preprint arXiv:2003.04297 (2020)
- [8] Chen, X., He, K.: Exploring simple siamese representation learning. In: CVPR (2021)
- [9] Chen, X., Xie, S., He, K.: An empirical study of training self-supervised vision transformers. In: CVPR (2021)
- [10] Coates, A., Ng, A., Lee, H.: An analysis of single-layer networks in unsupervised feature learning. In: Proceedings of the fourteenth international conference on artificial intelligence and statistics (2011)
- [11] contributors, I.: Imagenet terms of access (2020), <https://image-net.org/download>
- [12] Deng, J., Dong, W., Socher, R., Li, L.J., Li, K., Fei-Fei, L.: ImageNet: A Large-Scale Hierarchical Image Database. In: CVPR (2009)
- [13] Ermolov, A., Siarohin, A., Sangineto, E., Sebe, N.: Whitening for self-supervised representation learning. In: ICML (2021)
- [14] Everingham, M., Gool, L.V., Williams, C.K.I., Winn, J., Zisserman, A.: The pascal visual object classes (voc) challenge. International Journal of Computer Vision **88**, 303–308 (September 2009)
- [15] Fetterman, A., Albrecht, J.: Understanding self-supervised and contrastive learning with "bootstrap your own latent" (byol). Technical Report (2020)
- [16] Flickr, I.: Flickr terms and conditions of use (2020), <http://aiweb.techfak.uni-bielefeld.de/content/bworld-robot-control-software/>
- [17] Ghosh, A., Mondal, A.K., Agrawal, K.K., Richards, B.A.: Investigating power laws in deep representation learning. arXiv preprint arXiv:2202.05808 (2022)
- [18] Grill, J.B., Strub, F., Altché, F., Tallec, C., Richemond, P., Buchatskaya, E., Doersch, C., Avila Pires, B., Guo, Z., Gheshlaghi Azar, M., Piot, B., kavukcuoglu, k., Munos, R., Valko, M.: Bootstrap your own latent - a new approach to self-supervised learning. In: NeuralIPS (2020)
- [19] HaoChen, J.Z., Wei, C., Gaidon, A., Ma, T.: Provable guarantees for self-supervised deep learning with spectral contrastive loss. In: NeurIPS (2021)
- [20] He, B., Ozay, M.: Exploring the gap between collapsed and whitened features in self-supervised learning. In: ICML (2022)
- [21] He, K., Fan, H., Wu, Y., Xie, S., Girshick, R.: Momentum contrast for unsupervised visual representation learning. In: CVPR (2020)

- [22] He, K., Zhang, X., Ren, S., Sun, J.: Deep residual learning for image recognition. In: CVPR (2016)
- [23] Henaff, O.: Data-efficient image recognition with contrastive predictive coding. In: ICML (2020)
- [24] Hua, T., Wang, W., Xue, Z., Ren, S., Wang, Y., Zhao, H.: On feature decorrelation in self-supervised learning. In: ICCV (2021)
- [25] Huang, L., Yang, D., Lang, B., Deng, J.: Decorrelated batch normalization. In: CVPR (2018)
- [26] Huang, L., Zhao, L., Zhou, Y., Zhu, F., Liu, L., Shao, L.: An investigation into the stochasticity of batch whitening. In: CVPR (2020)
- [27] Jaiswal, A., Babu, A.R., Zadeh, M.Z., Banerjee, D., Makedon, F.: A survey on contrastive self-supervised learning. arXiv preprint arXiv:2011.00362 (2020)
- [28] Jing, L., Vincent, P., LeCun, Y., Tian, Y.: Understanding dimensional collapse in contrastive self-supervised learning. In: ICLR (2022)
- [29] Kessy, A., Lewin, A., Strimmer, K.: Optimal whitening and decorrelation. The American Statistician (2018)
- [30] Kingma, D.P., Ba, J.: Adam: A method for stochastic optimization. CoRR **abs/1412.6980** (2014)
- [31] Krizhevsky, A.: Learning multiple layers of features from tiny images. Tech. rep. (2009)
- [32] Le, Y., Yang, X.: Tiny imagenet visual recognition challenge. CS 231N (2015)
- [33] Li, C., Yang, J., Zhang, P., Gao, M., Xiao, B., Dai, X., Yuan, L., Gao, J.: Efficient self-supervised vision transformers for representation learning. In: ICLR (2022)
- [34] Li, J., Zhou, P., Xiong, C., Hoi, S.C.: Prototypical contrastive learning of unsupervised representations. In: ICLR (2021)
- [35] Lin, T.Y., Maire, M., Belongie, S., Hays, J., Perona, P., Ramanan, D., Dollar, P., Zitnick, L.: Microsoft coco: Common objects in context. In: ECCV (2014)
- [36] Liu, Y., Pan, S., Jin, M., Zhou, C., Xia, F., Yu, P.S.: Graph self-supervised learning: A survey. arXiv e-prints pp. arXiv–2103 (2021)
- [37] Oord, A.v.d., Li, Y., Vinyals, O.: Representation learning with contrastive predictive coding. arXiv preprint arXiv:1807.03748 (2018)
- [38] Ranasinghe, K., Naseer, M., Khan, S., Khan, F.S., Ryoo, M.: Self-supervised video transformer. In: CVPR (2022)
- [39] Richemond, P.H., Grill, J.B., Altché, F., Tallec, C., Strub, F., Brock, A., Smith, S., De, S., Pascanu, R., Piot, B., et al.: Byol works even without batch statistics. arXiv preprint arXiv:2010.10241 (2020)
- [40] Saunshi, N., Plevrakis, O., Arora, S., Khodak, M., Khandeparkar, H.: A theoretical analysis of contrastive unsupervised representation learning. In: ICML (2019)
- [41] Siarohin, A., Sangineto, E., Sebe, N.: Whitening and coloring batch transform for gans. In: ICLR (2019)
- [42] Tao, C., Wang, H., Zhu, X., Dong, J., Song, S., Huang, G., Dai, J.: Exploring the equivalence of siamese self-supervised learning via A unified gradient framework. In: CVPR (2022)
- [43] Tian, Y., Krishnan, D., Isola, P.: Contrastive multiview coding. In: European conference on computer vision (2020)
- [44] Tian, Y., Chen, X., Ganguli, S.: Understanding self-supervised learning dynamics without contrastive pairs. In: ICML (2021)

- [45] Tian, Y., Yu, L., Chen, X., Ganguli, S.: Understanding self-supervised learning with dual deep networks. CoRR **abs/2010.00578** (2020)
- [46] Vershynin, R.: High-dimensional probability: An introduction with applications in data science. Cambridge university press (2018)
- [47] Wu, Z., Xiong, Y., Yu, S.X., Lin, D.: Unsupervised feature learning via non-parametric instance discrimination. In: CVPR (2018)
- [48] Ye, M., Zhang, X., Yuen, P.C., Chang, S.F.: Unsupervised embedding learning via invariant and spreading instance feature. In: CVPR (2019)
- [49] Zbontar, J., Jing, L., Misra, I., Lecun, Y., Deny, S.: Barlow twins: Self-supervised learning via redundancy reduction. In: ICML (2021)
- [50] Zhang, C., Zhang, K., Zhang, C., Pham, T.X., Yoo, C.D., Kweon, I.S.: How does simsiam avoid collapse without negative samples? a unified understanding with self-supervised contrastive learning. In: ICLR (2022)
- [51] Zhang, H., Wu, Q., Yan, J., Wipf, D., Yu, P.S.: From canonical correlation analysis to self-supervised graph neural networks. In: NeurIPS (2021)
- [52] Zhang, S., Zhu, F., Yan, J., Zhao, R., Yang, X.: Zero-CL: Instance and feature decorrelation for negative-free symmetric contrastive learning. In: ICLR (2022)

A Details of Experimental Setup for Small and Medium Size Datasets

In this section, we provide the details of the implementation and training protocol for the experiments on small and medium size datasets (including CIFAR-10, CIFAR-100, STL-10, Tiny-ImageNet and ImageNet-100). Our implementation is based on the released codebase of *W-MSE* [13]⁶.

A.1 Datasets

The followings are the descriptions of 5 small and medium scale datasets, commonly used to evaluate the effectiveness of SSL models.

- CIFAR-10 and CIFAR-100 [31], two small-scale datasets composed of 32×32 images with 10 and 100 classes, respectively.
- STL-10 [10], derived from ImageNet [12], with 96×96 resolution images and more than 100K training samples.
- Tiny ImageNet [32], a reduced version of ImageNet [12], composed of 200 classes with images scaled down to 64×64 . The total number of images is: 100K (training) and 10K (testing).
- ImageNet-100 [43], a random 100-class subset of ImageNet [12].

A.2 Analytical Experiments

In section 3 of the submitted paper, we conduct several experiments on CIFAR-10 to illustrate our analysis. We provide a brief description of the setup in the caption of Figure 2 of the submitted paper. Here, we describe the details of these experiments. All experiments are uniformly based on the following training settings, unless otherwise stated in the figures of the submitted paper.

Training Settings We use the ResNet-18 as the encoder (dimension of *encoding* is 512.), a two layer MLP with ReLU and BN appended as the projector (dimension of the hidden layer and embedding are 1024 and 64 respectively). The model is trained on CIFAR-10 for 200 epochs with a batch size of 256, using Adam optimizer [30] with a learning rate of 3×10^{-3} , and learning rate warm-up for the first 500 iterations and a 0.2 learning rate drop at the last 50 and 25 epochs. The weight decay is set as 10^{-6} . All transformations are performed with 2 positives extracted per image with standard data augmentation (see Section A.3 for details). We use the same evaluation protocol as in *W-MSE* [13].

Method Settings In the experiments shown in Figure 2 and Figure 4 of the paper, fully PCA whitening suffers the dimensional collapse and further produces numerical instability. Therefore, we use the MSE loss without L2 normalization and partition its channel dimension into 4 groups, which makes it possible to finish training in a normal way. Despite the reduced setting for whitening, PCA whitening still has problems as shown in Figure 2 and Figure 4. In other experiments, we use the MSE loss with L2 normalization for all methods, as *W-MSE* [13] does.

A.3 Experimental Setup for Comparison of Baselines

In section 4.1 of the paper, we compare our channel whitening with random group partition (CW-RGP) to the state-of-the-art SSL methods on CIFAR-10, CIFAR-100, STL-10 and Tiny-ImageNet datasets. Here, we describe the training details of these experiments. Except for the hyper-parameters relating to CW-RGP itself (*e.g.*, the group number), our experimental setups are strictly following the setup of the *W-MSE* [13] paper, as following descriptions.

Encoder and Projector We use the ResNet-18 [22] as the encoder and the dimension of *encoding* is 512. We use a 2-layers MLP as the projector: one hidden layer with BN and Relu applied to it and a linear layer as output. In the experiments of CIFAR-10, CIFAR-100 and STL-10, the dimension of the hidden layer in the projector and *embedding* are 1024 and 512, respectively. In the experiments of Tiny-ImageNet, the dimension of the hidden layer in the projector and *embedding* are 2048 and 1024, respectively.

⁶<https://github.com/htdt/self-supervised>

Image Transformation Details We make the image transformation following the details in [6], which extract crops with a random size from 0.2 to 1.0 of the original area and a random aspect ratio from 3/4 to 4/3 of the original aspect ratio. The horizontal mirroring is applied with a probability of 0.5. The color jittering configuration is (0.4, 0.4, 0.4, 0.1) with a probability of 0.8 and grayscaling with a probability of 0.1. For ImageNet-100, the crop size is from 0.08 to 1.0, jittering is strengthened to (0.8, 0.8, 0.8, 0.2), grayscaling probability is 0.2, and Gaussian blurring is with a probability of 0.5. We use only one crop at testing time in all the experiments (standard protocol).

Optimizer and Learning Rate Schedule We use the Adam optimizer [30]. We apply the same number of epochs and learning rate schedule to all the compared methods. Specifically, for CIFAR-10 and CIFAR-100, we use 1,000 epochs with a learning rate of 3×10^{-3} ; for STL-10, 2,000 epochs with a learning rate of 2×10^{-3} ; for Tiny-ImageNet, 1000 epochs with a learning rate of 2×10^{-3} . In these experiments, we use a 0.2 learning rate drop at the last 50 and 25 epochs. The weight decay is 10^{-6} . In all experiments, we use learning rate warm-up for the first 500 iterations of the optimizer. We use a batch size of 512 for CW-RGP 2 in CIFAR-100, STL-10 and Tiny ImageNet experiments, while 256 for the others.

Evaluation Protocol We use the same setup of evaluation protocol as in W-MSE [13]: training the linear classifier for 500 epochs using the Adam optimizer and the labeled training set of each specific dataset, without data augmentation; the learning rate is exponentially decayed from 10^{-2} to 10^{-6} and the weight decay is 5×10^{-6} . In addition, we also evaluate the accuracy of a k-nearest neighbors classifier (k-NN, $k = 5$) in these experiments.

For our CW-RGP, we denote ‘RGP₂’ to indicate CW using random group partition, with a group number of 2. We find that our CW-RGP can also work well when batch-slicing, proposed in W-MSE [13], is used. We thus also use batch slicing (a default setting in the released code of W-MSE) to ensure that the channel number is larger than the batch size for our CW-RGP. In the experiments of CIFAR-10, CIFAR-100 and STL-10, we use RGP₄ and the slicing sub-batch size is 64. In the experiments of Tiny-ImageNet, we use RGP₂ and the slicing sub-batch size is 128.

For a fair comparison, we also reproduce several related methods (including SimSiam [8], Barlow Twins [49], VICReg [2], and Zero-ICL [52]) under the same training and evaluation settings as in [13]. However, These methods using the configuration of hyper-parameters based on the original baselines in [13] get poor results in our training mode (e.g, a 2-layers projector, using Adam optimizer [30], ‘step’ learning rate schedule, and so on). In the reproduction experiments, we use the recommended 2048-2048-2048 projector for these methods which obtains significantly better results than the default 1024-512 or 1024-64 projector in [13]. In particular, for Barlow Twins [49], we set the trade-off coefficient λ to 0.0078 instead of the recommended 0.0051 in [49], since that using the recommended 0.0051 has a significant degenerated performance in our experiments. For SimSiam [8], we use the SGD optimizer and cosine learning rate schedule as recommended in [8], because the loss value fluctuates sharply and it leads to very poor results when we use Adam optimizer for the training. We conjecture that the optimization mechanism of Adam may be not suitable for the training of predictor in SimSiam [8]. Other settings not mentioned here are the same as in [13] by default.

B Proofs

B.1 proof of $\frac{\partial \mathcal{L}}{\partial \theta} = \frac{\partial \mathcal{L}'}{\partial \theta}$.

As stated in Section 3.3 of the paper, given one mini-batch input \mathbf{X} with two augmented views, we say the loss:

$$\mathcal{L}(\mathbf{X}) = \frac{1}{m} \|\widehat{\mathbf{Z}}_1 - \widehat{\mathbf{Z}}_2\|_F^2. \quad (13)$$

and the proxy loss:

$$\mathcal{L}'(\mathbf{X}) = \frac{1}{m} \|\widehat{\mathbf{Z}}_1 - (\widehat{\mathbf{Z}}_2)_{st}\|_F^2 + \frac{1}{m} \|(\widehat{\mathbf{Z}}_1)_{st} - \widehat{\mathbf{Z}}_2\|_F^2, \quad (14)$$

has the same gradients w.r.t. the learnable parameters θ , i.e., $\frac{\partial \mathcal{L}}{\partial \theta} = \frac{\partial \mathcal{L}'}{\partial \theta}$. Here, we provide the proof.

Proof. Note that $\widehat{\mathbf{Z}}_1$ and $\widehat{\mathbf{Z}}_2$ are the function of θ . Based on the chain rule, we have:

$$\begin{aligned}\frac{\partial \mathcal{L}}{\partial \theta} &= \frac{\partial \frac{1}{m} \|\widehat{\mathbf{Z}}_1 - \widehat{\mathbf{Z}}_2\|_F^2}{\partial \theta} \\ &= \frac{1}{m} \frac{\partial \|\widehat{\mathbf{Z}}_1 - \widehat{\mathbf{Z}}_2\|_F^2}{\partial \widehat{\mathbf{Z}}_1} \frac{\partial \widehat{\mathbf{Z}}_1}{\partial \theta} + \frac{1}{m} \frac{\partial \|\widehat{\mathbf{Z}}_1 - \widehat{\mathbf{Z}}_2\|_F^2}{\partial \widehat{\mathbf{Z}}_2} \frac{\partial \widehat{\mathbf{Z}}_2}{\partial \theta}.\end{aligned}\quad (15)$$

Similarly, we have:

$$\begin{aligned}\frac{\partial \mathcal{L}'}{\partial \theta} &= \frac{\partial (\frac{1}{m} \|\widehat{\mathbf{Z}}_1 - (\widehat{\mathbf{Z}}_2)_{st}\|_F^2 + \frac{1}{m} \|(\widehat{\mathbf{Z}}_1)_{st} - \widehat{\mathbf{Z}}_2\|_F^2)}{\partial \theta} \\ &= \frac{1}{m} \frac{\partial \|\widehat{\mathbf{Z}}_1 - (\widehat{\mathbf{Z}}_2)_{st}\|_F^2}{\partial \widehat{\mathbf{Z}}_1} \frac{\partial \widehat{\mathbf{Z}}_1}{\partial \theta} + \frac{1}{m} \frac{\partial \|(\widehat{\mathbf{Z}}_1)_{st} - \widehat{\mathbf{Z}}_2\|_F^2}{\partial \widehat{\mathbf{Z}}_2} \frac{\partial \widehat{\mathbf{Z}}_2}{\partial \theta} \\ &= \frac{1}{m} \frac{\partial \|\widehat{\mathbf{Z}}_1 - \widehat{\mathbf{Z}}_2\|_F^2}{\partial \widehat{\mathbf{Z}}_1} \frac{\partial \widehat{\mathbf{Z}}_1}{\partial \theta} + \frac{1}{m} \frac{\partial \|\widehat{\mathbf{Z}}_1 - \widehat{\mathbf{Z}}_2\|_F^2}{\partial \widehat{\mathbf{Z}}_2} \frac{\partial \widehat{\mathbf{Z}}_2}{\partial \theta}.\end{aligned}\quad (16)$$

From Eqn. 15 and Eqn. 16, we have $\frac{\partial \mathcal{L}}{\partial \theta} = \frac{\partial \mathcal{L}'}{\partial \theta}$. \square

B.2 Proof of Proposition 1

As stated in Section 3.3 of the paper, by looking into the first term of Eqn. 14, we aim to minimize the following objective:

$$\min_{\mathbf{Z}_1} \mathcal{L}'_1(\mathbf{Z}_1) = \min_{\mathbf{Z}_1} \frac{1}{m} \|\phi(\mathbf{Z}_1)\mathbf{Z}_1 - (\widehat{\mathbf{Z}}_2)_{st}\|_F^2. \quad (17)$$

Here, $\phi(\mathbf{Z}_1)$ is the whitening matrix that depends on \mathbf{Z}_1 , and $\widehat{\mathbf{Z}}_2$ is a whitened matrix with $\frac{1}{m} \widehat{\mathbf{Z}}_2 \widehat{\mathbf{Z}}_2^T = \mathbf{I}$. We prove the following Proposition.

Proposition 2. *Let $\mathbb{A} = \arg \min_{\mathbf{Z}_1} \mathcal{L}'_1(\mathbf{Z}_1)$. We have that \mathbb{A} is not an empty set, and $\forall \mathbf{Z}_1 \in \mathbb{A}$, \mathbf{Z}_1 is full-rank. Furthermore, for any $\{\sigma_i\}_{i=1}^{d_z}$ with $\sigma_1 \geq \sigma_2 \geq \dots, \sigma_{d_z} > 0$, we construct $\widetilde{\mathbb{A}} = \{\mathbf{Z}_1 | \mathbf{Z}_1 = \mathbf{U}_2 \text{diag}(\sigma_1, \sigma_2, \dots, \sigma_{d_z}) \mathbf{V}_2^T$, where $\mathbf{U}_2 \in \mathbb{R}^{d_z \times d_z}$ and $\mathbf{V}_2 \in \mathbb{R}^{m \times d_z}$ are from the singular value decomposition of $\widehat{\mathbf{Z}}_2$, i.e., $\mathbf{U}_2(\sqrt{m}\mathbf{I})\mathbf{V}_2^T = \widehat{\mathbf{Z}}_2$. When we use ZCA whitening, we have $\widetilde{\mathbb{A}} \subseteq \mathbb{A}$.*

Proof. Based on the fact that $\mathcal{L}'_1 \geq 0$, we have $\mathbb{A} = \{\mathbf{Z}_1 | \mathcal{L}'_1(\mathbf{Z}_1) = 0\}$. It is easy to validate that $\mathcal{L}'_1(\widehat{\mathbf{Z}}_2) = 0$, and we have $\widehat{\mathbf{Z}}_2 \in \mathbb{A}$. Therefore, \mathbb{A} is not an empty set.

We then prove that $\forall \mathbf{Z}_1 \in \mathbb{A}$, \mathbf{Z}_1 is full-rank. We assume that for any $\mathbf{Z}_1 \in \mathbb{A}$ and \mathbf{Z}_1 is not a full-rank matrix, i.e., $\text{Rank}(\mathbf{Z}_1) < d_z$. We have $\text{Rank}(\phi(\mathbf{Z}_1)\mathbf{Z}_1) \leq \text{Rank}(\mathbf{Z}_1) < d_z$. We thus have that $\phi(\mathbf{Z}_1)\mathbf{Z}_1$ is not a full-rank matrix. Therefore, it is impossible for $\phi(\mathbf{Z}_1)\mathbf{Z}_1 = \widehat{\mathbf{Z}}_2$ since $\widehat{\mathbf{Z}}_2$ is a full-rank matrix. So $\mathcal{L}'_1(\mathbf{Z}_1) > 0$, which is contradictory to $\mathbf{Z}_1 \in \mathbb{A}$. Therefore, we have $\forall \mathbf{Z}_1 \in \mathbb{A}$, \mathbf{Z}_1 is full-rank.

For any $\{\sigma_i\}_{i=1}^{d_z}$ with $\sigma_1 \geq \sigma_2 \geq \dots, \sigma_{d_z} > 0$, let $\mathbf{Z}_1 = \mathbf{U}_2 \text{diag}(\sigma_1, \sigma_2, \dots, \sigma_{d_z}) \mathbf{V}_2^T$, we now prove that $\phi(\mathbf{Z}_1)\mathbf{Z}_1 = \widehat{\mathbf{Z}}_2$ when using ZCA whitening. We know $\phi(\mathbf{Z}_1) = \Phi_{ZCA} = \mathbf{U}\Lambda^{-\frac{1}{2}}\mathbf{U}^T$, where $\Lambda = \text{diag}(\lambda_1, \dots, \lambda_{d_z})$ and $\mathbf{U} = [\mathbf{u}_1, \dots, \mathbf{u}_{d_z}]$ are the eigenvalues and associated eigenvectors of the covariance matrix Σ of \mathbf{Z}_1 . We know $\Sigma = \frac{1}{m} \mathbf{Z}_1 \mathbf{Z}_1^T = \mathbf{U}_2 \text{diag}(\sigma_1^2/m, \sigma_2^2/m, \dots, \sigma_{d_z}^2/m) \mathbf{U}_2^T$. Since the eigen decomposition of Σ is unique, we have $\phi(\mathbf{Z}_1) = \mathbf{U}_2 \text{diag}(\sqrt{m}/\sigma_1, \sqrt{m}/\sigma_2, \dots, \sqrt{m}/\sigma_{d_z}) \mathbf{U}_2^T$. Therefore, $\phi(\mathbf{Z}_1)\mathbf{Z}_1 = \mathbf{U}_2 \text{diag}(\sqrt{m}/\sigma_1, \sqrt{m}/\sigma_2, \dots, \sqrt{m}/\sigma_{d_z}) \mathbf{U}_2^T \mathbf{U}_2 \text{diag}(\sigma_1, \sigma_2, \dots, \sigma_{d_z}) \mathbf{V}_2^T = \mathbf{U}_2(\sqrt{m}\mathbf{I})\mathbf{V}_2^T = \widehat{\mathbf{Z}}_2$. We thus have $\widetilde{\mathbb{A}} \subseteq \mathbb{A}$. \square

C Algorithm of CW-RPG

We describe our CW-RGP algorithm in Py-Torch style code, shown in Figure 8.

```
def channel_whitening(x, gamma, beta, g, eps=1e-5):
    # x: input feature with size [m, d] or [m, d, H, W]
    # gamma, beta: the trainable affine
    # g: the group number of group whitening
    x_flatten = x.view(x.size()[0], -1)
    f_dim = x_flatten.size()[-1]
    shuffle = torch.randperm(f_dim).tolist()
    # centering
    mean = x_flatten.mean(-1, keepdim=True)
    x_centered = x_flatten - mean
    x_group = x_centered[:, shuffle].reshape(x.size()[0], g, -1).permute(1, 2, 0)
    f_cov = torch.bmm(x_group.permute(0, 2, 1), x_group) / (x_group.shape[1] - 1)
    eye = torch.eye(x.size(0)).type(x.type()).reshape(1, x.size(0), x.size(0)).repeat(g, 1, 1)
    # compute whitening matrix
    sigma = (1 - eps) * f_cov + eps * eye
    u, eig, _ = sigma.svd()
    scale = eig.rsqrt()
    wm = torch.bmm(u, torch.diag_embed(scale))
    wm = torch.bmm(wm, u.permute(0, 2, 1))
    # whiten
    decorrelated = torch.bmm(x_group, wm)
    shuffle_recover = [shuffle.index(i) for i in range(f_dim)]
    decorrelated = decorrelated.permute(2, 0, 1).reshape(-1, f_dim)[:, shuffle_recover]
    output = decorrelated.view_as(x)
    return output * gamma + beta
```

Figure 8: Py-Torch style code of CW-RPG.

D Details of Experiments for Large-Scale Classification and Transfer Learning

In this section, we provide the details of implementation and training protocol for the experiments on large-scale ImageNet [12] classification, and transfer learning to VOC [14] object detection, COCO [35] object detection and instance segmentation.

D.1 Datasets

- ImageNet [12], the well-known largescale dataset with about 1.3M training images and 50K test images, spanning over 1000 classes.
- VOC07+12 [14], the PASCAL Visual Object Classes Challenge. VOC2007: 20 classes with 9,963 images containing 24,640 annotated objects; VOC2012: 20 classes with 11,530 images containing 27,450 ROI annotated objects and 6,929 segmentations.
- COCO2017 [35], a large-scale object detection, segmentation, and captioning dataset with 330K images containing 1.5 million object instances.

D.2 Experiment on ImageNet

In section 4.1 of the paper, we compare our CW-RGP to the state-of-the-art SSL methods on large-scale ImageNet classification. Here, we describe the training details of these experiments. Our implementation is based on the released codebase of *SimSiam* [8]⁷. Except for the hyper-parameters relating to CW-RGP itself, we strictly follow the setup of the SimSiam paper [8].

Encoder and Projector We use the ResNet-50 [22] as the encoder and the dimension of *encoding* is 2048. We use a 3-layers MLP as the projector: two hidden layers with BN and Relu applied to it and a linear layer as output. The dimension of the hidden layer and embedding are 2048 and 1024, respectively.

Image Transformation Details In image transformation, we follow the details in [8]: crop size from 0.2 to 1.0, no strengthened jittering (0.4, 0.4, 0.4, 0.1) with probability 0.8, grayscaling probability 0.2, and Gaussian blurring with 0.5 probability. We use standard protocol at testing time.

Optimizer and Learning Rate Schedule We apply the SGD optimizer, using a learning rate of $lr \times \text{BatchSize} / 256$ with a base lr of 0.05 and cosine decay schedule. The weight decay is 10^{-4} and the SGD momentum is 0.9. In addition, we use learning rate warm-up for the first 500 iterations of the optimizer. We only try the batch size of 256 and 512 due to memory limitation.

Evaluation Protocol We use the same setup of evaluation protocol as in *Simsiam* [8]: training the *linear classifier* for 100 epochs with the *LARS* optimizer (using a learning rate of $lr \times \text{BatchSize} / 256$ with a base lr of 0.1 and cosine decay schedule). The batch size for evaluation is 1024.

For our CW-RGP, we use RGP_2 for CW. We find that our CW-RGP can also work well when combined with the whitening penalty (covariance loss) used in VICReg [2]. For adapting to the sample orthogonalization in CW, we use a covariance loss along the channel dimension (see Section F for details). We empirically set the weight of covariance loss as 0.001 for the half training epochs to amplify the extent of whitening, which obtains a top-1 accuracy of 69.7% when training 100 epochs, compared to 69.6% of the method using CW-RGP only. Here, we address that our CW-RGP can combine with covariance loss to obtain good results. We believe the performance can be further improved, if we fine-tune the weight of covariance loss.

D.3 Experiments for Transfer Learning

In this part, we describe the training details of experiments for transfer learning. Our implementation is based on the released codebase of *MoCo* [21]⁸ for transfer learning to object detection and instance

⁷<https://github.com/facebookresearch/simsiam> under the CC-BY-NC 4.0 license.

⁸<https://github.com/facebookresearch/moco/tree/main/detection> under the CC-BY-NC 4.0 license.

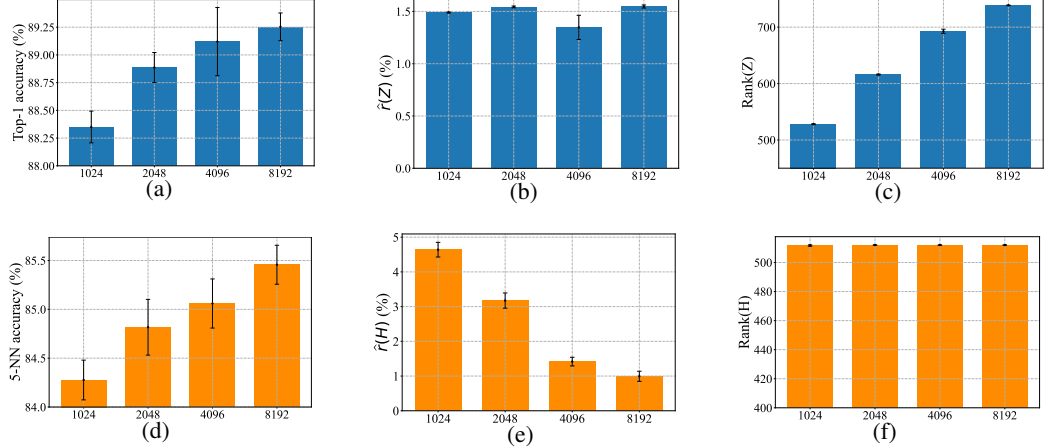


Figure 9: Illustration of different projectors when varying the dimension of the hidden layer. We show (a) the linear accuracies; (b) the normalized stable-rank of *embedding*; (c) the rank of *embedding*. (d) the k-NN accuracies; (e) the normalized stable-rank of *encoding*; (f) the rank of *encoding*. All results are averaged by five random seeds, with standard deviation shown as error bars.

segmentation tasks. We use the default hyper-parameter configurations from the training scripts provided by the codebase for CW-RGP, using our 200-epoch pre-trained model on ImageNet.

For the experiments of ‘VOC 07+12 detection’, we use Faster R-CNN fine-tuned in VOC 2007 trainval + 2012 train, evaluated in VOC 2007 test. For the experiments of ‘COCO detection and COCO instance segmentation’, we use Mask R-CNN (1× schedule) fine-tuned in COCO 2017 train, evaluated in COCO 2017 val. All Faster/Mask R-CNN models are with the C4-backbone. Our CW-RGP is performed with 3 random seeds, with mean and standard deviation reported.

E Investigating the Projector MLP

As mentioned in section 5 of the submitted paper, we conduct preliminary experiments to explore how the projector affects the extents of whitening between *encoding* and *embedding*. Specifically, we conduct experiments to explore the extents of whitening between *encoding* and *embedding* by varying the dimension and number of the hidden layer of the projector, based on our CW-RGP algorithm.

Dimension of the Hidden Layer Here, we conduct experiments on *CIFAR-10* to observe the effect by using different dimensions, ranging in $\{1024, 2048, 4096, 8192\}$, of the hidden layer. In the experiments, we set the projector: one hidden layer with BN and Relu applied to it and a linear layer as output (the *embedding* is 2048). We train the model for 200 epochs (other settings are the same as the experiments described in Section A.2). We use *encoding* as the representation for evaluation. The results are shown in Figure 9. We observe that CW-RGP can obtain improved linear/5-NN accuracy, and increased rank of *embedding*, when increasing the dimension of the hidden layer. We find that CW-RGP can make the *encoding* full-rank for all settings with different dimensions. Besides, there are no significant differences in terms of the stable-rank (the extent of whitening) of *embedding* for all settings. One interesting observation is that the stable-rank of *encoding* decreases as the dimension of the hidden layer increases. For this observation, we conjecture that the large hidden-layer dimension may amplify the largest eigenvalue of the covariance matrix of *encoding* (driven by back-propagation), which leads to the decrease of stable-rank of *encoding*.

Number of the Hidden Layer We then conduct experiments on *Tiny ImageNet* to observe the effect by using different numbers, ranging in $\{1, 2, 3, 4, 5\}$, of the hidden layer (dimension of the hidden layer and embedding are 2048 and 1024 respectively). We train the model for 400 epochs (other settings are the same as the experiments described in Section A.2). We use *encoding* as the representation for evaluation. The results are shown in Figure 10. We observe that CW-RGP can obtain increased rank and stable-rank (extent of whitening) of *embedding*, when decreasing the numbers of the hidden layer from 5 to 2. We also find that CW-RGP can make the *encoding* to be full-rank for almost all settings with different numbers of the hidden layer, except that CW-RGP

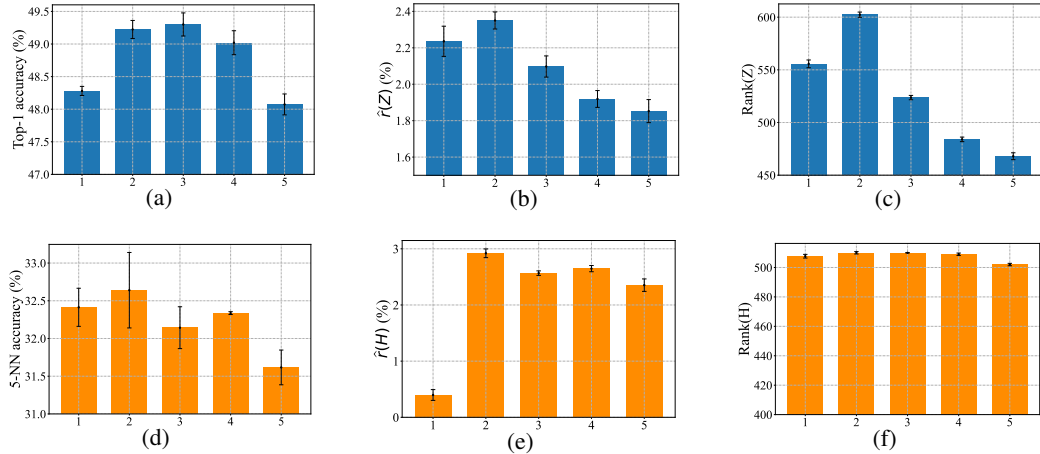


Figure 10: Illustration of different projectors when varying the number of the hidden layer. We show (a) the linear accuracies; (b) the normalized stable-rank of *embedding*; (c) the rank of *embedding*. (d) the k-NN accuracies; (e) the normalized stable-rank of *encoding*; (f) the rank of *encoding*. All results are averaged by three random seeds, with standard deviation shown as error bars.

with the projector using 5 hidden-layer has slightly reduced rank and has slightly worse performance. For this experiment, we do not obtain a clear clue that how the numbers of the hidden layer of the projector affects the extent of whitening.

F Covariance Loss along Channel Dimension

We note that VICReg [2] uses covariance loss along the batch dimension to constrain the evolution of the covariance matrix of *embedding* \mathbf{Z} to a diagonal matrix. The main idea is to reduce the value of non-diagonal elements of the covariance matrix. It is natural to extend this covariance loss along the channel dimension and we explore whether covariance loss can be used together with whitening loss in this section.

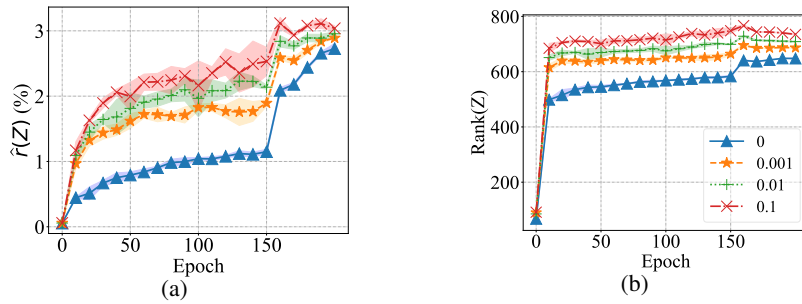


Figure 11: Illustration of CW with different penalty weights $\{0, 0.001, 0.01, 0.1\}$ of the covariance loss. We use the ResNet-18 as the encoder (dimension of representation is 512.), a two layer MLP with ReLU and BN appended as the projector (dimension of embedding is 2048). The model is trained on CIFAR-10 for 200 epochs with a batch size of 256 and standard data argumentation, using Adam optimizer [30] (more details of experimental setup please see Section A). We show (a) the normalized stable-rank of *embedding*; (b) the rank of *embedding*. The results are averaged by five random seeds, with standard deviation shown using shaded region.

For adapting to the sample orthogonalization like our channel whitening (CW), we propose a covariance loss along the channel dimension as follows:

$$\text{Centering} : \mathbf{Z}_c = (\mathbf{I} - \frac{1}{d}\mathbf{1}\cdot\mathbf{1}^T)\mathbf{Z}, \quad (18)$$

$$\text{Covariance matrix} : \Sigma = \frac{1}{d-1}\mathbf{Z}_c^T\mathbf{Z}_c, \quad (19)$$

$$\text{Covariance loss} : C = \frac{1}{m} \sum_{i \neq j} \Sigma_{i,j}^2, \quad (20)$$

We conduct experiments to show that our CW can work well with the covariance loss and the covariance loss even can amplify the extent of whitening of the embedding. We use CW combining the covariance loss with varying penalty weights ranging in $\{0, 0.001, 0.01, 0.1\}$. The results are shown in Figure 11. We observe that CW can obtain a significantly higher rank and stable-rank of *embedding* \mathbf{Z} , when increasing the penalty weight of covariance loss, especially in the early stage of training where a relatively large learning rate is used. We also note that CW with covariance loss using a penalty weight of 0.001 obtains an accuracy of 88.78%, slightly better than CW without covariance loss which has an accuracy of 88.50%.

G Licenses of Datasets

ImageNet [12] is subject to the ImageNet terms of access [11].

PASCAL VOC [14] uses images from Flickr, which is subject to the Flickr terms of use [16].

The annotations of COCO [35] are under the Creative Commons Attribution 4.0 License. The images are subject to the Flickr terms of use [16].